Transient dielectric functions of Ge, Si, and InP from femtosecond pump-probe ellipsometry

Transient dielectric functions of Ge, Si, and InP from femtosecond pump-probe ellipsometry

Cite as: Appl. Phys. Lett. **115**, 052105 (2019); doi: 10.1063/1.5109927
Submitted: 14 May 2019 · Accepted: 1 July 2019 ·
Published Online: 1 August 2019

Shirly Espinoza,[1,a)] Steffen Richter,[1,2] Mateusz Rebarz,[1] Oliver Herrfurth,[2] Rüdiger Schmidt-Grund,[2] Jakob Andreasson,[1,3] and Stefan Zollner[4,5,b)]

AFFILIATIONS

[1]ELI Beamlines, Fyzikální ústav AV ČR, v.v.i., Za Radnicí 835, 25241 Dolní Břežany, Czech Republic
[2]Universität Leipzig, Felix-Bloch-Institut für Festkörperphysik, Linnéstr. 5, 04103 Leipzig, Germany
[3]Department of Physics, Chalmers University of Technology, Kemigården 1, 41296 Gothenburg, Sweden
[4]Fyzikální ústav AV ČR, v.v.i., Sekce optiky, Na Slovance 2, CZ-18221 Praha 8, Czech Republic
[5]Department of Physics, New Mexico State University, P.O. Box 30001, Las Cruces, New Mexico 88003, USA

[a)]**Email:** shirly.espinoza@eli-beams.eu
[b)]**Email:** zollner@nmsu.edu. **URL:** http://ellipsometry.nmsu.edu

ABSTRACT

Transient dielectric functions with a 120 fs time resolution of Ge, Si, and InP were acquired from 1.7 to 3.5 eV with a femtosecond pump-probe rotating-compensator ellipsometer. The intensity of the pump laser (with 1.55, 3.10, or 4.65 eV photon energy) was adjusted to create an initial near-surface carrier density of $10^{20}\,\mathrm{cm}^{-3}$. In Ge, there is a significant (∼15%) decrease in the E_1 and $E_1+\Delta_1$ critical point absorption and a Kramers–Kronig consistent change in the refractive index because photoexcited electrons at L block these transitions and reduce their amplitudes. Only a small redshift of the E_1 critical point is observed, which we attribute to lattice heating and exchange-correlation effects. Minimal changes were found for Si and InP, where electrons near Δ and Γ do not participate in interband transitions between 1.7 and 3.5 eV.

Transient effects in semiconductors[1] occur on multiple time scales from femtoseconds (10^{-15} s) to microseconds (10^{-6} s), spanning many orders of magnitude. They govern the performance of electronic and optoelectronic devices,[2] including transistors, detectors, and lasers. The corresponding matrix elements for the related scattering processes[2,3] enter the Boltzmann[4] or semiconductor Bloch equations.[5–7] The dielectric function[6] (DF) of a semiconductor determines its absorption, transmission, and reflection properties. It depends on the distribution functions of electrons, holes, and acoustic as well as optical phonons. Excitation with an intense quasimonochromatic femtosecond laser pulse changes these distributions and therefore makes the DF dependent on the pump-probe delay time and probe photon energy.

Taking advantage of recent improvements in femtosecond pump-probe ellipsometry[8,9] with a continuum white light probe beam, we measured the transient dielectric functions of Ge, Si, and InP from 1.7 to 3.5 eV after excitation with a femtosecond pump pulse of 1.55, 3.10, and 4.65 eV photon energy. These three semiconductors have similar valence band structures formed by p-bonding orbitals, but their conduction bands[10] lead to different transient responses.

In Ge, a nearly direct elemental semiconductor, excitation by 1.55 eV pulses produces a uniformly high density of electrons and holes throughout the probed crystal volume near the center of the Brillouin zone, see Fig. 1. The electrons quickly scatter to the L- and X-minima in the conduction band. Our DF data show how L-valley electrons affect the amplitudes and energies of the E_1 and $E_1+\Delta_1$ peaks due to band filling and bandgap renormalization (BGR). (The E_1 and $E_1+\Delta_1$ critical points arise from a van Hove singularity in the joint density of states in diamond and zinc blende semiconductors,[10] because the two highest valence bands are parallel to the lowest conduction band along the Λ-direction of the Brillouin zone.) The DF changes are consistent with the Kramers–Kronig relations between the real and imaginary parts. Comparison with higher-energy pump pulses and with Si and InP confirms our interpretation.

In our experiments (Fig. 2), an amplified Ti:sapphire laser (Coherent Astrella) produced 35 fs pump pulses at 800 nm with a 1 kHz repetition rate and a pulse energy of 6 mJ. A small fraction (∼1 μJ) of the fundamental beam was diverted and focused on a rotating 2 mm thick CaF_2 platelet to generate white light continuum probe pulses. The

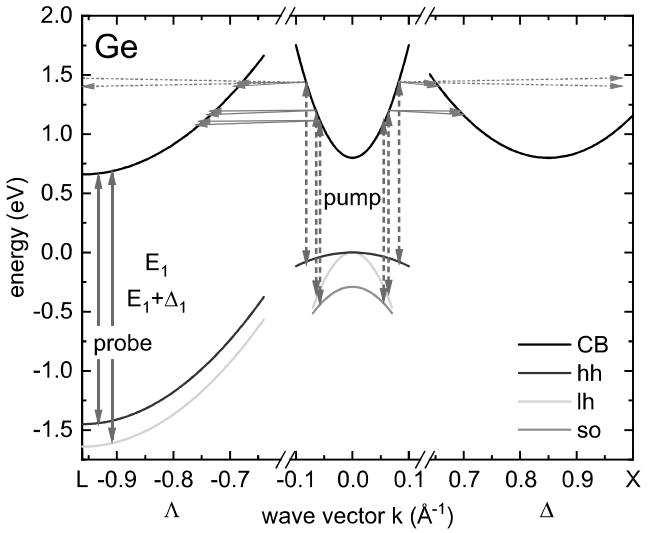

FIG. 1. Schematic band structure of Ge (ignoring nonparabolicity and warping) showing optical interband transitions (red) from the heavy (hh), light (lh), and split-off (so) hole bands into the conduction band (CB) with 1.55 eV photoexcitation. Electron-phonon coupling with multiple phonon modes (magenta) scatters the electrons to the *L*- and *X*-valleys, where they relax.

main part of the beam provided pump pulses at 800, 400, or 267 nm (generated by frequency doubling or tripling). Their intensity could be adjusted with a variable neutral density filter. Ellipsometry measurements[11] were performed in the polarizer-sample-rotating compensator-analyzer (PSC_RA) configuration. The probe beam was focused on the sample (diameter $<200\,\mu$m) by a spherical mirror with a 20 cm focal length at an incident angle of 60° with respect to the surface normal and then passed through a wire grid polarizer (Thorlabs).

The s-polarized pump pulses had an incidence angle of 45° and were focused onto the sample ($1/e^2$ diameter $\sim350\,\mu$m) to overlap with the probe beam. The delay between pump and probe pulses was

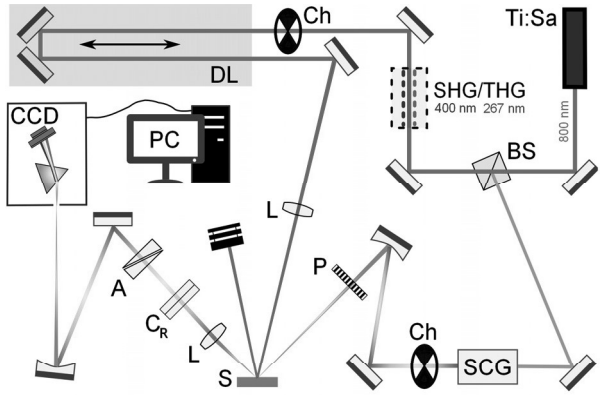

FIG. 2. Experimental setup of the femtosecond pump-probe spectroscopic rotating-compensator ellipsometer. Ch, chopper; A, analyzer; P, wire-grid polarizer; C_R, rotating compensator; L, lens; S, sample; DL, delay line; BS, beam splitter; SHG/THG, second/third harmonic generation (optional), SCG, super-continuum generation; and CCD, charge-coupled device detector. A photograph is shown in Fig. S1.

controlled by an optical delay line based on a high precision linear translation stage (Newport). The reflected probe beam was collimated and transmitted through a superachromatic quarter wave plate compensator (Halle) and a Glan-Taylor prism analyzer (Thorlabs). The polarizer and analyzer were fixed at ±45°, while the compensator was rotated in ten steps of 50° each. Reflectance spectra for each probe pulse were recorded by a detection system consisting of a charged-coupled device (CCD) camera with submillisecond readout (Entwicklungsbüro Stresing) and a prism spectrograph. For each compensator position j and for each pump-probe delay, reflectance-difference spectra $(\Delta R/R)_j$ were averaged over 500 probe pulses to reduce the effects of intensity fluctuations of the white-light continuum.

Using two choppers in the pump and probe beams enabled correction of ambient and pump-related background (including photoluminescence, Rayleigh scattering, and second-harmonic generation). In addition, spectra taken without the pump were compared with reference measurements on a steady-state commercial ellipsometer to correct systematic errors.[9] The pump-probe spectra for short time delays (<1 ps) were corrected for the group velocity dispersion (chirp) introduced mainly by the wire grid polarizer and the CaF_2 plate. The temporal and spectral resolutions were 120 fs and 5 nm, respectively.

Our experimental design has significant advantages[9] over single-wavelength time-resolved ellipsometry[12–14] or multiple-angle polarized reflectance[15,16] and does not rely on a specific dielectric function model.[17]

Since the probe area easily fits inside the pump area, we can neglect the radial symmetry of the experiment and assume homogeneous planar excitation without lateral diffusion. For an 800 nm pump beam, the penetration depth in bulk Ge is 220 nm, while it ranges from 10 to 60 nm for probe photon energies between 2.0 and 3.5 eV, much smaller than the pump penetration depth. Therefore, the Ge volume reflecting the probe beam has a uniform initial carrier concentration of $10^{20}\,\mathrm{cm}^{-3}$ for an 800 nm pump beam with an incident areal energy density of 2 mJ/cm^2 per pulse.[9] (Static values of the optical constants were used to estimate the initial carrier concentration. Transient bleaching at the pump wavelength will decrease the absorption, while a decrease in the refractive index will reduce reflection losses.) We can thus ignore the depth-dependence of the dielectric function and directly convert the ellipsometric angles (Fig. 3) into a transient pseudodielectric function, see Fig. 4.

Within the first 500 fs, we see a steady decrease in the amplitudes of the E_1 and $E_1+\Delta_1$ transitions[18] in $\langle\epsilon_2\rangle$ for Ge, accompanied by a small redshift of E_1 (but not $E_1+\Delta_1$). These peaks do not change much from 500 fs to 2 ps and then recover. Full recovery takes about 500 ps, except that the E_1 and $E_1+\Delta_1$ broadenings are still smaller after 4 ns than initially. For a 2.6 eV probe energy (above $E_1+\Delta_1$), the recovery is much faster. It starts at 500 fs delay time and is completed after 2 ps. At the highest probe energies above 3 eV, the time-dependence of $\langle\epsilon_2\rangle$ is weak. Below 2 eV, a blue-shift of the rising slope of $\langle\epsilon_2\rangle$ below E_1 during the first 2 ps is difficult to distinguish from the E_1 amplitude decrease. Changes in $\langle\epsilon_1\rangle$ over time are related to the $\langle\epsilon_2\rangle$ changes by Kramers–Kronig transform. For example, the low-energy limit of $\langle\epsilon_1\rangle$ decreases within the first 2 ps as the E_1 amplitude decreases.

The corresponding changes for Si and InP (see Figs. S11 and S5 in the supplementary material) for the 800 nm pump with the same electron-hole concentration of $10^{20}\,\mathrm{cm}^{-3}$ are much smaller. We conclude that the origin for the large changes in the transient dielectric

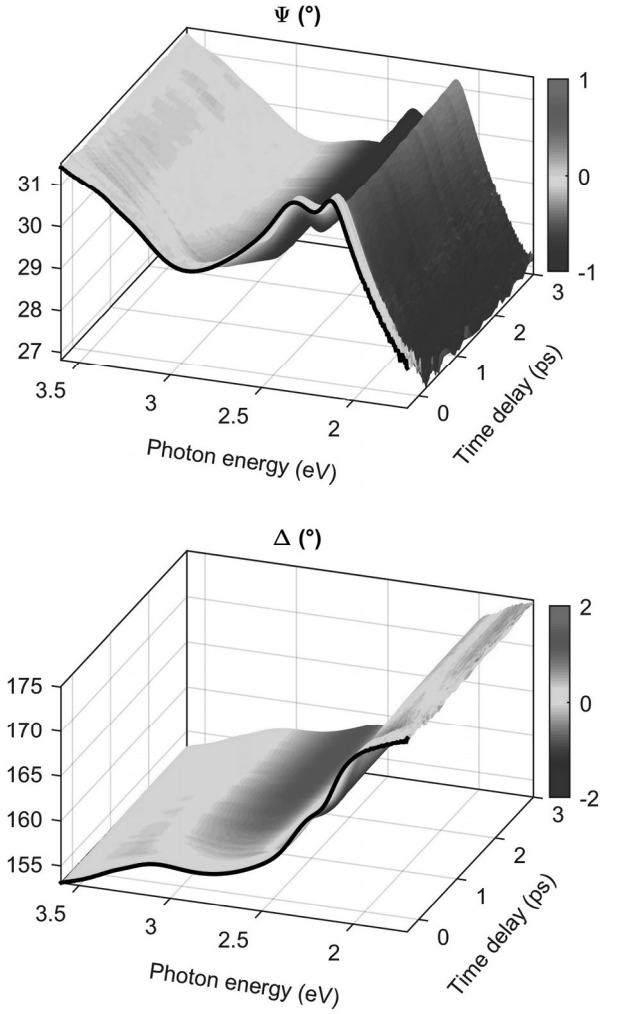

FIG. 3. Transient ellipsometric angles ψ and Δ for bulk Ge (covered by a 4.5 nm thick native oxide) at a 60° angle of incidence with a 1.55 eV pump (10^{20} cm^{-3} carrier concentration) as a function of photon energy and pump-probe delay time. Increases relative to the initial spectra before excitation (black) are shown in red and decreases are shown in blue.

function of Ge after the 800 nm pump are due to its peculiar band structure, where the conduction band minimum is at the L-point.[10]

The temperature increase inside the probed Ge volume exposed to one pump pulse can be estimated from $\Delta T = E(1 - R)/cV\rho$ to be on the order of 25 K, where $E = 2.9$ μJ is the incident pump pulse energy, $R = 0.54$ the reflectance of the pump pulse, $V = 3 \times 10^{-8}$ cm^3 the excited volume, $c = 0.32$ J/g K the specific heat of Ge, and $\rho = 5.3$ g cm^{-3} its density. (Radiative recombination will reduce this temperature increase.) The temperature dependence of the E_1 energy is about –0.4 meV/K (see Ref. 18), and therefore, we expect an E_1 red-shift due to heating of no more than 10 meV. The observed redshift, while difficult to quantify, is about 20 meV. We conclude that heating is responsible for a significant portion of the observed redshift. On the other hand, it is difficult to explain why heating affects E_1 and $E_1 + \Delta_1$ differently, since Δ_1 is independent of temperature and doping.[19,20]

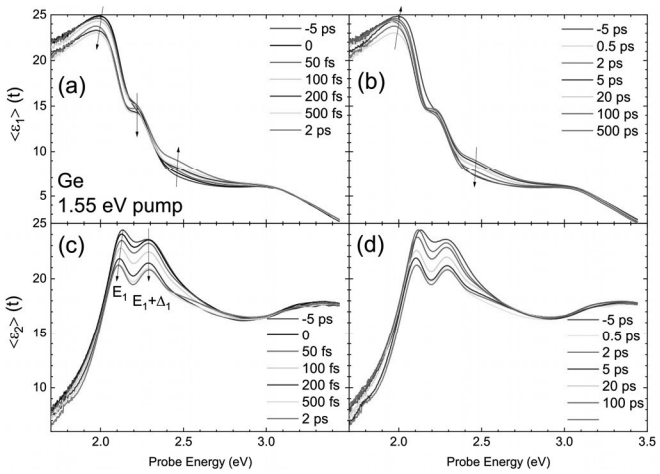

FIG. 4. Real (top) and imaginary (bottom) parts of the transient pseudodielectric function of Ge (with 4.5 nm native oxide) vs photon energy near the E_1 and $E_1 + \Delta_1$ transitions during the first 2 ps (left) and at later times (right) after photoexcitation of 10^{20} cm^{-3} electron-hole pairs with a pump photon energy of 1.55 eV.

In the discussion of our Ge results, we neglect screening of the E_1 excitons by the high carrier concentration because it is not important for Ge: the E_1 and $E_1 + \Delta_1$ peaks in Ge are much less affected by excitonic effects than in Si or GaAs.[21] It is known that the E_1 and $E_1 + \Delta_1$ amplitudes in Ge are much less reduced by doping than in Si.[20,22] Band-filling[20] dominates exciton screening.

We explain the evolution of the transient pseudodielectric function of Ge after excitation with 800 nm pump pulses in reference to Fig. 1: the 1.55 eV pump photons excite three different electron-hole populations through interband transitions originating from the heavy, light, and split-off hole bands. The excess energy of these electrons (heavy holes) is up to 0.6 eV (0.1 eV), which would correspond to electron and heavy hole temperatures of 4600 and 800 K, respectively.

Through the electron-phonon deformation potential interaction,[23] some electrons quickly scatter to the L-valleys, where the density of states is ten times higher than in the Γ-valley. There are four different phonon modes at the L-point (transverse and longitudinal acoustic and optical phonons), all of which contribute to the scattering processes, because the selection rules are only valid at high-symmetry points.[23] Due to the small transverse electron mass at the L-point (out of the plane of the figure), a broad range of transitions is possible (dotted lines in Fig. 1). The electrons will populate several ellipsoidal energy surfaces in $\vec{k}$-space around the four L-points. Due to the large scattering vector for these processes, intervalley scattering is not screened by the photoexcited carriers, see the supplementary material. Even more electrons, however, scatter into the X-valleys, where the density of states is even higher than in the L-valleys. The transfer of electrons from the Γ- to the L- or X-valleys requires only one scattering process by a single phonon with a time scale of less than 50 fs, i.e., below our time resolution.[24] The photoexcited holes, on the other hand, have insufficient energy to scatter to the L-point and therefore remain near Γ.

The transient pseudodielectric function of Ge with 50 fs time delay is similar to the steady-state spectra. This means that nearly 10^{20} cm^{-3} electrons in the X-valley and a similar number of holes near Γ have only a small impact on the pseudodielectric function between

1.7 and 3.5 eV because they do not participate in the E_1 and $E_1 + \Delta_1$ transitions. Many-body effects are local in $\vec{k}$-space.[25] Only carriers with a wave vector $\vec{k}_0$ can renormalize transitions at $\vec{k}_0$. Therefore, electrons at X and holes at Γ cannot impact the E_1 transitions at L and along Λ.

Subsequently, the carriers form thermal Fermi-Dirac distributions and cool down by phonon emission (mostly deformation-potential scattering because the Fröhlich interaction does not exist in a nonpolar semiconductorlike Ge).[1,3,10] Within 500 fs, they scatter from the X-valley to the L-valley, which has about 0.4 eV less energy. The nonequilibrium electron distribution in the L-valley partially blocks the E_1 and $E_1 + \Delta_1$ transitions (Pauli blocking), thus reducing the amplitude of the E_1 and $E_1 + \Delta_1$ peaks in the pseudodielectric function (Fig. 4).

Because the electron temperature is still very high after 500 fs, Pauli blocking extends beyond 2.6 eV. At 2 ps, the electrons have cooled down significantly, and therefore, the pseudodielectric function at 2.6 eV has recovered its equilibrium value. On the other hand, the carrier density at L has not changed much yet, indicated by the reduced amplitudes of the E_1 and $E_1 + \Delta_1$ peaks.

Between 2 ps and 500 ps, the E_1 and $E_1 + \Delta_1$ amplitudes of Ge recover. This means that the electron concentration falls below the measureable threshold, first by the highly nonlinear Auger recombination and later by ambipolar diffusion and electron-hole pair (radiative or nonradiative) recombination. The next pump pulse arrives after 1 ms, much longer than the recombination or diffusion time.

We note that the broadenings of the E_1 and $E_1 + \Delta_1$ peaks in Ge do not change much with time, only their amplitude. These broadenings are mostly due to the lifetime of holes near the L-point and not affected by the electrons.[26] Therefore, they do not depend on the delay time.

The E_1 peak of $\langle \epsilon_2 \rangle$ in Ge redshifts by no more than 20 meV, while the $E_1 + \Delta_1$ peak does not redshift at all. This limits the magnitude of BGR, which seems to be of the same order of magnitude as laser heating. The redshift might also indicate that the $\Lambda_{4,5}$ and Λ_6 valence bands are not exactly parallel to the corresponding Λ_6 conduction bands.[20] Because of the large density of final states available for the E_1 and $E_1 + \Delta_1$ transitions, we do not expect a Burstein-Moss shift due to Pauli blocking, only a reduction of the peak amplitudes.[27]

The redshift due to BGR in doped semiconductors has three contributions: (1) the self-energy due to the breaking of the translational crystal symmetry by ionized impurity atoms,[22] (2) the correlation hole due to Coulomb repulsion, and (3) Pauli exclusion.[25] While all three of these are present in doped Ge, only the latter two occur under high photoexcitation. For the E_1 gap in n-type Ge with an electron concentration of $10^{20}\,\mathrm{cm}^{-3}$, a BGR redshift of 61 meV was found,[20] much larger than the redshift seen in our experiments at the same electron-hole concentration. We conclude that the main contribution to the BGR redshift in doped semiconductors is impurity disorder scattering, not exchange-correlation effects.

In summary, we observe significant changes due to band filling in the femtosecond transient dielectric function of Ge near the E_1 and $E_1 + \Delta_1$ transitions, but not for Si and InP. The difference is explained by the conduction band structure of these materials, where the minimum is located at L, Δ, and Γ, respectively. There is also a small redshift of these critical points due to laser induced lattice heating and many-body effects (bandgap renormalization).

See the supplementary material for experimental results with discussion for Si and InP and data acquired with 3.1 and 4.65 eV pump photon energy, while this manuscript focuses on the results for Ge with 1.55 eV pump pulses.

This work was supported by the European Regional Development Fund (Projects ADONIS Reg. No. CZ.02.1.01/0.0/0.0/16 019/0000789 and ELIBIO Reg. No. CZ.02.1.01/0.0/0.0/15 003/0000447) and by Deutsche Forschungsgemeinschaft, SFB 762-Projektnr. 31047526 (Project B03), the National Science Foundation (No. DMR-1505172), the European Union Structural and Investment Funds, and the Czech Ministry of Education, Youth, and Sports (National Programme of Sustainability II and CZ.02.2.69/0.0/0.0/16_027/0008215, Project IOP Researchers Mobility). OH acknowledges support from the Leipzig School of Natural Sciences—Building with Molecules and Nano-objects and JA from the Chalmers Area of Advanced Materials Science.

REFERENCES

[1] J. Shah, *Ultrafast Spectroscopy of Semiconductors and Semiconductor Nanostructures* (Springer, Berlin, 1999).
[2] K. Hess, *Monte Carlo Device Simulation: Full Band and Beyond* (Kluwer, New York, 1991).
[3] L. Reggiani, *Hot-Electron Transport in Semiconductors* (Springer, Berlin, 1985).
[4] N. W. Ashcroft and N. D. Mermin, *Solid State Physics* (Saunders, Fort Worth, 1976).
[5] H. Haug and S. W. Koch, *Quantum Theory of the Optical and Electronic Properties of Semiconductors*, 4th ed. (World Scientific, Singapore, 2004).
[6] C. Klingshirn, *Semiconductor Optics* (Springer, Berlin, 2005).
[7] M. Lindberg and S. W. Koch, Phys. Rev. B **38**, 3342 (1988).
[8] M. Rebarz, M. Kloz, S. J. Espinoza Herrera, and C. D. Brooks, *UV-VIS-NIR Femtosekundovy Elipsometricky System*, utility model 30838, Czech Republic, 2017.
[9] S. Richter, O. Herrfurth, S. Espinoza, M. Rebarz, M. Kloz, J. A. Leveillee, A. Schleife, S. Zollner, M. Grundmann, J. Andreasson, and R. Schmidt-Grund, e-print arXiv:1902.05832v1.
[10] P. Y. Yu and M. Cardona, *Fundamentals of Semiconductors* (Springer, Berlin, 2010).
[11] H. Fujiwara, *Spectroscopic Ellipsometry* (Wiley, Chichester, 2007).
[12] D. H. Auston and C. V. Shank, Phys. Rev. Lett. **32**, 1120 (1974).
[13] G. E. Jellison and D. H. Lowndes, Appl. Opt. **24**, 2948 (1985).
[14] H. Choo, X. Hu, M. C. Downer, and V. Kesan, Appl. Phys. Lett. **63**, 1507 (1993).
[15] L. Huang, J. P. Callan, E. N. Glezer, and E. Mazur, Phys. Rev. Lett. **80**, 185 (1998).
[16] C. A. D. Roeser, A. M.-T. Kim, J. P. Callan, L. Huang, E. N. Glezer, Y. Siegal, and E. Mazur, Rev. Sci. Instrum. **74**, 3413 (2003).
[17] C. J. Kaplan, P. M. Kraus, A. D. Ross, M. Zürch, S. K. Curshing, M. F. Jager, H.-T. Chang, E. M. Gullikson, S. M. Neumark, and S. R. Leone, Phys. Rev. B **97**, 205202 (2018).
[18] L. Viña, S. Logothetidis, and M. Cardona, Phys. Rev. B **30**, 1979 (1984).
[19] N. S. Fernando, T. N. Nunley, A. Ghosh, C. M. Nelson, J. A. Cooke, A. A. Medina, S. Zollner, C. Xu, J. Menendez, and J. Kouvetakis, Appl. Surf. Sci. **421**, 905 (2017).
[20] C. Xu, J. Kouvetakis, and J. Menéndez, J. Appl. Phys. **125**, 085704 (2019).
[21] P. Lautenschlager, M. Garriga, L. Viña, and M. Cardona, Phys. Rev. B **36**, 4821 (1987).
[22] L. Viña and M. Cardona, Phys. Rev. B **34**, 2586 (1986).
[23] S. Zollner, S. Gopalan, and M. Cardona, J. Appl. Phys. **68**, 1682 (1990).
[24] S. Zollner, S. Gopalan, and M. Cardona, Solid State Commun. **76**, 877 (1990).
[25] H. Kalt and M. Rinker, Phys. Rev. B **45**, 1139 (1992).
[26] P. Lautenschlager, P. B. Allen, and M. Cardona, Phys. Rev. B **33**, 5501 (1986).
[27] C. Xu, N. S. Fernando, S. Zollner, J. Kouvetakis, and J. Menéndez, Phys. Rev. Lett. **118**, 267402 (2017).